The 2014 World Congress on
Advances in Civil, Environmental, and Materials Research (ACEM14)
Busan, Korea, August 24-28, 2014

Evaluation of the strength of elastically-supported glass plates for wind-resistance design of windows

*Daisuke Konno[1)], Eri Gavanski[2)] and Yasushi Uematsu[3)]

[1), 2),3)] *Department of Architecture and Building Science, Tohoku University, Japan*
[1)] *konno-d@hjogi.pln.archi.tohoku.ac.jp*

ABSTRACT

Strength and failure characteristics of elastically-supported glass plates are examined by performing full-scale breakage tests and numerical simulation which can predict glass failure pressure. In full-scale breakage tests, three types of wind loading were applied to the specimens, including dynamic loading created based on wind tunnel measurement, up to plate failure. The results are consistent with the assumption that the damage accumulation of glass is independent of loading patterns. In addition, the numerical simulation, which was originally developed for simply-supported glass plates, was modified so that it can be applicable to glass plates elastically supported. The effects of several input parameters for the numerical simulation on the calculate failure pressure were investigated in order to choose the best combination of these parameters for closely replicating the full-scale breakage test results.

1. INTRODUCTION

Glass failure due to wind loading is caused by static fatigue, which is a time-dependent reduction of strength after the application of a certain duration of load (Minor 1981), and this needs to be considered for window design. Brown's integral as shown in Eq.(1) (Brown 1972;1974) is a theoretical equation used to capture the static fatigue;

$$DA'_{crit} = \int_0^{t_f} \left[p(t) \right]^s dt \tag{1}$$

[1)] Graduate Student
[2)] Assistant Professor
[3)] Professor

where t_f is failure time, $p(t)$ is applied pressure, s is a coefficient (generally its value is determined as 10 to 20 (Brown 1972; Dalgliesh 1979; Kawabata 1996; Gavanski 2009)), and DA'_{crit} is damage accumulation at the critical crack on a glass surface. Eq.(1) indicates that glass failure occurs when the damage accumulation reaches its critical value.

Since the magnitude of damage accumulation, DA'_{crit}, expressed in Eq.(1), becomes too large to evaluate with ease, this figure is usually converted into an equivalent load, which was historically used to examine load resistance capacities (Holmes 1985; Kanabolo and Norville 1985; Reed 1993; Li et al. 1999; Ko et al. 2005). The way to convert from DA'_{crit} into equivalent loads is shown in Eq.(2);

$$p_{eq}\left(t_{ref}\right) = \left\{ \int_0^T \left[p(t) \right]^s dt \Big/ t_{ref} \right\}^{1/s} = \left(DA / t_{ref} \right)^{1/s} \tag{2}$$

where p_{eq} is equivalent load, t_{ref} is reference time, and T is time of predicted wind loading histories in design situation.

In order to perform this conversion on glass specimen, DA'_{crit}, expressed in Eq.(1), must be independent of loading pattern. Gavanski (2009) showed that Brown's integral is independent of loading pattern for glass plates which are simply supported at their edges by conducting full-scale breakage tests.

However, glass plates used in actual buildings are not simply supported but elastically supported by gasket at their edges (denoted as "elastic support condition" hereafter). Therefore, it is necessary that the independence of DA'_{crit} of loading pattern needs to be proved for the elastic support condition.

Considering the background presented above, present study will performe full-scale breakage tests using glass plates with elastic support condition in order to examine the validity of Brown's integral as well as to capture glass plate behavior under wind loadings. Furthermore, the numerical simulation which can predict glass failure pressure, originally developed by Simiu and Reed (1983; 1984), and employed by Kawabata (1996) and Gavanski (2009), will be modified so that it can be applicable for elastically-supported glass plates.

2. FULL-SCALE BREAKAGE TESTS

2.1 EXPERIMENTAL APPARATUS AND PROCEDURES

In order to apply dynamic wind pressure, "Pressure Loading Actuator" (PLA), developed at University of Western Ontario (UWO), shown in Fig.1, was employed in the present study. This loading device can replicate realistic, full-scale, temporally-varying wind pressure. For details, the reader is referred to Kopp et al. (2010).

In present study, monolithic annealed window glass plates whose size of 855mm×790mm×3mm, shown in Fig.2, were selected as test specimens. The edges of glass plate are clamped with gasket and covered with aluminum frames as illustrated in Fig.3. This edge condition will be referred as elastic support condition and allows the glass plate to move in plane and out-of-plane and to rotate along the plate edge.

Each glass specimen was mounted in a pressure box connected to PLA with a

hose (Fig.4), in order to apply wind pressure. On the front face of this box, a plywood panel fastened with several bolts acts as the support for the aluminum frames which hold the glass specimen in place. Only negative pressures were applied so that most of broken glasses get into the inside of pressure box for safety. Moreover, it is known that initial strength of glass plate has a great deal of variation because it is directly related to a surface condition of glass plate, and its variation affects full-scale breakage test results (Gavanski 2009). Therefore, the window specimens which were produced in same production line, delivered/preserved in same way, and paid close attention to their handling were prepared with a corporation of a window manufacturing company.

Fig.1 Pressure Loading Actuator

Fig. 2 Window specimen

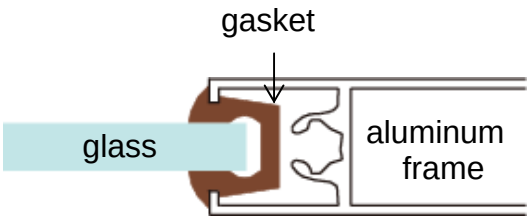

Fig.3 Illustration of glass plate support

Fig.4 Pressure Box with window specimen

2.2 TEST CONFIGURATIONS

Three types of pressure traces were applied on specimens until glass failure, viz., 2 ramp loadings (Ramp1, Ramp2) and realistic dynamic loading (Dynamic). For each loading pattern, 20 specimens were utilized.

Two ramp loading rates were chosen to be consistent with those used by Miyoshi (1964) and Gavanski (2009). “Ramp1” is a lower loading rate (16.4(Pa/sec)), and “Ramp2” is a higher loading rate (230(Pa/sec)). In ramp loading tests, failure pressure and failure time were recorded for comparing the results and coefficient *s* necessary for Brown's integral was calculated.

Dynamic loading (Dynamic) was created using the wind pressure coefficient (C_p) time series obtained from wind tunnel test with a low-rise residential building. Area

averaged wind pressure coefficients, C_{pA}, whose tributary area is the same as the one for window specimen and calculated using the tributary area method of Kopp et al. (2005), were obtained for all walls of a testing model (B×D×H=9m×10m×8m) for all wind directions. The location of window and wind direction which experience the largest C_{pA} was selected. With C_{pA} time series corresponding to this window location and the wind direction, wind pressure time histories ($p(t)$) were calculated using the following equation;

$$p(t) = 0.5\rho V_f{}^2 C_{pA}(t) \tag{3}$$

where V_f is reference wind speed and ρ is air density. V_f =50(m/sec) was selected to correspond with the maximum design wind speed in Japan specified in the AIJ Recommendations . Since, C_p is referenced with dynamic wind pressure measured as 10(min) mean wind speed at a height of 10(m) in open country terrain, V_f needs to correspond to this. Consequently, $p(t)$ created in this way was employed as the input pressure trace for dynamic loading.

If specimen does not break at the end of the application of this pressure trace, it would have been desirable to keep applying the same pressure trace repeatedly until failure, as was done in Gavanski (2009). However, we have decided to recalculate the input pressure trace with increased V_f by 3(m/sec) and to apply the same specimen in order to perform the test with relatively short testing time. The glass failure is evaluated using DA'_{crit} instead of the actual failure pressure level. In addition, the purpose of the present tests was to examine whether different loading patterns affect the glass failure, i.e., DA'_{crit}. Hence, it is believed that the current method is still appropriate for the purpose of this testing. It is noted that the pressure time histories for each scaling wind speed were applied sequentially, with no pause for changes in V_f. Fig.5 provides an example of an entire pressure time series that were applied to a specimen. Points when V_f changes are indicated by a change in color.

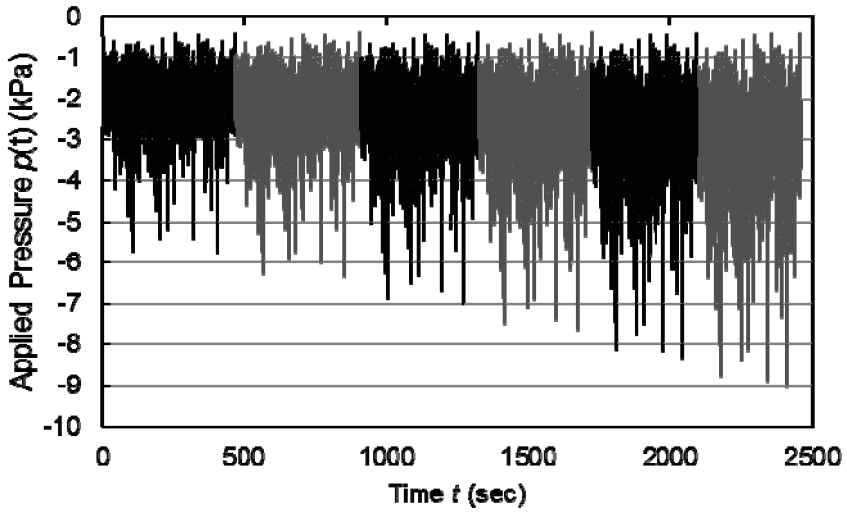

Fig.5 Time histories of Dynamic that used in tests.

2.3 TEST RESULTS

General observations Table.1 presents test results of all loading patterns. Failure pressure, p_f, is the pressure applied at the moment of failure, as measured by a pressure transducer attached to the pressure box. Simple mean, p_{f_mean}, maximum, p_{f_max}, minimum, p_{f_min}, standard deviation, *S.D*, and coefficient of variation, *COV,* of failure pressure among 20 specimens are calculated and shown in Table 1. Compared to the typical *COV* values of glass strength of 0.22 (Beason 1980), those obtained for the present test are relatively small (0.10~0.12), indicating less variability in failure pressure. p_f for faster loading (Ramp 2) is larger than those for slower loading (Ramp 1), and this is consistent with the characteristic expected from Eq.(1), that is, the effect of a change in loading rate on glass.

With respect to dynamic loading (Dynamic), it cannot be evaluated by failure pressure since a same pressure level can occur at different time steps, meaning that failure pressure cannot represent damage accumulation amount. Hence, equivalent load, p_{eq_3sec}, expressed using Eq.(2), is presented for comparing with other loading patterns. Reference time of 3(sec) was used, and coefficient *s* of 17 was used (the choice of *s* value will be described in the next section). As a result, p_{eq_3sec} for Dynamic seems to be larger than those for ramp loadings. The possible reason for this difference will be discussed later.

Table.1 Statistics of failure pressure and equivalent load

		Ramp1	Ramp2	Dynamic
Loading Rate	(Pa/sec)	16.4	230	n/a
The # of specimens	(-)	20	20	20
Temperature Range	(°C)	19-22	19-23	11-28
Humidity Range	(%)	38-55	42-66	4-22
p_{f_mean}	(kPa)	7.48	8.66	n/a
p_{f_max}	(kPa)	8.74	10.38	n/a
p_{f_min}	(kPa)	5.78	6.71	n/a
S.D	(kPa)	0.92	0.89	n/a
COV	(-)	0.12	0.10	n/a
$p_{eq\_3sec\_mean}$	(kPa)	8.47	8.45	9.88
$p_{eq\_3sec\_max}$	(kPa)	9.99	10.26	11.38
$p_{eq\_3sec\_min}$	(kPa)	6.42	6.45	6.84
S.D	(kPa)	1.11	0.92	1.14
COV	(-)	0.13	0.11	0.12

Calculation of Brown's integral coefficient *s* In order to convert damage accumulation into equivalent load, the coefficient, *s*, in Eq.(1) should be evaluated. The value of *s* is known to vary between 10 to 20 (Brown 1972; Dalgliesh 1979; Kawabata 1996; Gavanski 2009) depending on glass type, glass geometry, critical crack location as well as other factors. Thus, it was necessary to evaluate *s* from test results. Assuming that Brown's integral is independent of loading rate, i.e., damage accumulations from two ramp loadings are equal, which will be proved in the following section, Eq.(1) can be converted into Eq.(4);

$$DA'_{crit1} = DA'_{crit2}$$

$$\therefore \frac{\ln(p_{f1}) - \ln(p_{f2})}{\ln(p'_1) - \ln(p'_2)} = \frac{1}{s+1} \tag{4}$$

where *p'* is loading rate. Eq.(4) shows a relationship between failure pressures, p_f, and loading rates, *p'*, and Fig.6 presents this relationship using the present test results. The coefficient, *s*, was obtained to be about 17 using ensemble averages of 20 failure pressure from two ramp loading test results. This value is in the range of *s* value obtained in previous studies and this indicates the validity of present test results.

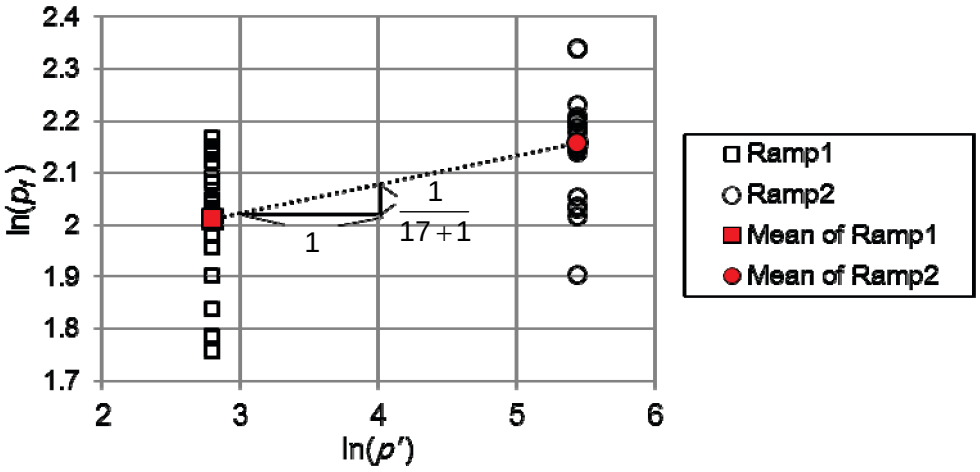

Fig. 6 Determination of Brown's integral coefficient *s*

Validity of Brown's integral In order to present the validity of Brown's integral among different loading patterns, the damage accumulation, DA'_{crit}, needs to be compared using the present test results. However since its figure tends to be large, equivalent loads expressed as shown in Eq.(2) was calculated instead. In present study, equivalent loads for all loading patterns were calculated by using coefficient *s*=17 that was obtained in the previous section. The reference time, t_{ref}, was necessary for the calculation of equivalent load and was set to be 3(sec).

Fig.7 shows cumulative distribution function (CDF) of 3-sec equivalent load,

p_{eq_3sec}, for all loading patterns. The failure probability was plotted by Thomas method;

$$F = \frac{i}{N+1} \tag{5}$$

where *F* is failure probability, *i* is the rank of specimen when they are in ascendant order and *N* is the total number of specimens. As a numerical integration performed for calculating damage accumulations, Simpson's rule was applied as shown in Eq.(6);

$$\begin{aligned} DA'_{crit} &= \int_0^{t_f} [p(t)]^s dt \\ &= \frac{h}{3}\left\{ [p(0)]^s + 4\sum_{i=1}^{\frac{n}{2}} [p(t_{2i-1})]^s + 2\sum_{i=1}^{\frac{n}{2}-1} [p(t_{2i})]^s + [p(t_f)]^s \right\} \end{aligned} \tag{6}$$

where *h* is divided width among sampling data.

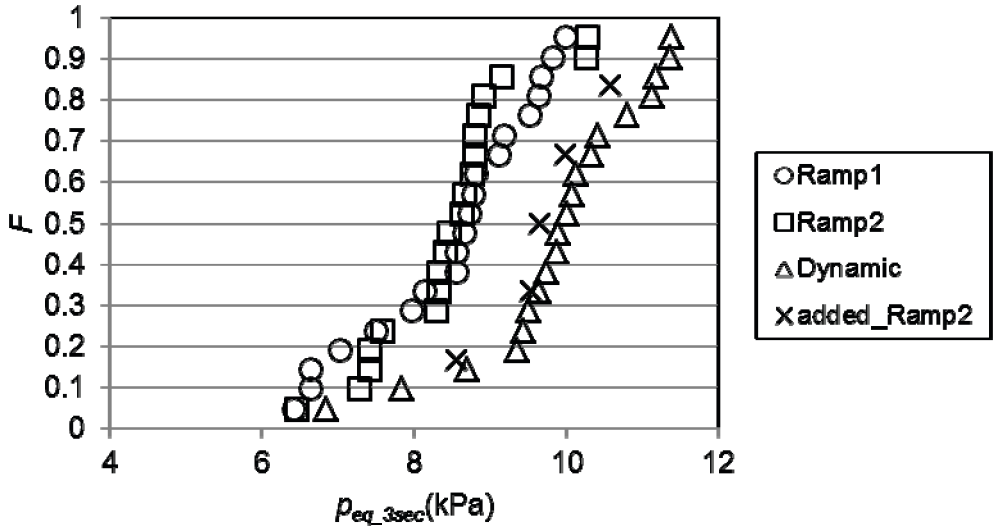

Fig.7 CDFs of 3-sec equivalent load.

The CDFs of both ramp loadings correspond reasonably well. By using a Kolmogorov-Smirnov test, it was found that the null hypothesis of the difference between these loading patterns as being zero cannot be rejected by using a 95% confidence interval. However, the CDF of Dynamic does not follow those of ramp loadings at all probability levels.

The reason for this discrepancy is likely to be the effect of humidity. As shown in Table.1, the humidity during the ramp loading tests was much higher than the one during the Dynamic test (the ramp loading tests were performed first and 2 month later, the Dynamic test was performed, which was in December). Wiederhorn (1967) mentions that the strength of glass decreases when humidity increases because the water promotes the growth of crack at a glass surface. Consequently, glass plate failure was

delayed for the dynamic loading test compared to the ramp loading test and this resulted in larger p_{eq_3sec} for Dynamic.

In order to examine this hypothesis, an additional experiment was carried out, denoted as added_Ramp2, under the testing condition where humidity is as low as those when Dynamic test was performed. Since there are only 5 glass plates left which were manufactured in the same production line as others used for the test, added_Ramp2 was performed with only 5 specimens, instead of 20. The p_{eq_3sec} of added_Ramp2 is bigger than those of other ramp loading tests, and the CDF of p_{eq_3sec} from added_Ramp2 shows a similar trend to the one from Dynamic regardless of a small number of test specimens. By using a Kolmogorov-Smirnov test, it was found that the null hypothesis of the difference as zero cannot be rejected by using a 95% confidence interval. Hence, the difference in p_{eq_3sec} between the Dynamic and ramp loadings seems to have been caused by the difference in humidity. Since the number of specimen utilized was small, the presented results may not be sufficient enough to validate Brown's integral. However, we can conclude at least that results which disagree with the applicability of Brown's integral to ramp and dynamic loadings have not been found in the present study and the further analysis will be performed assuming this validity.

3. NUMERICAL SIMURATION

There is a numerical simulation method for predicting failure pressure of glass plate subjected to wind loading, originally suggested by Simiu and Reed (1983; 1984) and utilized by Kawabata (1996). In this simulation method, Simiu and Reed used fracture mechanics in order to obtain time-dependent glass strength. Gavanski (2009) performed comparisons between numerical simulation results and full-scale breakage test results, assuming plates are simply-supported and modified the original simulation method for its improvement.

In the present study, we attempt to modify this numerical simulation so that we can use this for the glass plates whose edges are elastically supported.

3.1 METHODOLOGY

The methodology of the numerical simulation is briefly explained herein. For further details, the reader is referred to Gavanski (2009). The time-dependent glass strength of an element on a glass plate at location M_j, which contains a crack oriented normal to α_k after t (sec) of load application is described as;

$$S(M_j,\alpha_k,t)=\left[\left\{S_i\left(M_j,\alpha_k\right)\frac{K_{IC}}{K_{Ii}}\right\}^{n-2}-\frac{n-2}{2}AY^2K_{IC}^{n-2}\int_0^{t_f}\sigma_a^n(M_j,\alpha_k,t)dt\right]^{\frac{1}{n-2}} \tag{7}$$

where S_i (M_j, α_k) is the initial strength of an element at point M_j that contains a crack oriented normal to α_k. K_{IC} is a fracture toughness; K_{Ii} is an initial stress intensity factor; Y is a geometrical shape factor; A and n are crack growth coefficients; and σ_a is the stress at location (M_j, α_k) after t (sec) of load application.

The value of S_i (M_j, α_k) is generated using the Monte-Carlo technique assuming that S_i (M_j, α_k) follows the Weibull distribution as shown in Eq.(8);

$$P\left(S_i,A',\alpha_1<\alpha<\alpha_2\right)=1-\exp\left\{-\left(\frac{S_i\left(M_j,\alpha_k\right)}{S_0(A',\alpha_1<\alpha<\alpha_2)}\right)^m\right\} \tag{8}$$

where P (S_i, A', $\alpha_1<\alpha<\alpha_2$) is the probability of the initial strength of an element whose area is A' and which contains a crack having an orientation angle of $\alpha_1<\alpha<\alpha_2$, $S_0(A', \alpha_1<\alpha<\alpha_2)$ is a scale parameter, and m is a shape parameter. $S_0(A', \alpha_1<\alpha<\alpha_2)$ and m were obtained by conducting ring-on-ring tests with small glass plate specimens.

The value of σ_a (M_j, α_k, t) can be expressed as;

$$\sigma_a\left(M_j,\alpha_k,t\right)=\sigma_x\left(M_j,t\right)\cos^2\alpha_k+\sigma_y\left(M_j,t\right)\sin^2\alpha_k+2\tau_{xy}\left(M_j,t\right)\sin\alpha_k\cos\alpha_k \tag{9}$$

where $\sigma_x(M_j, t)$ and $\sigma_y(M_j, t)$ are normal stress, and $\tau_{xy}(M_j, t)$ is shear stress at the each element location M_j on the glass surface calculated by Finite Element Method (FEM) analysis further explained in the next section.

By comparing the strength expressed in Eq.(7) and the stress expressed in Eq.(9) at each location, M_j, direction, α_k, and time, t, the failure is defined as the moment when the relationship expressed in Eq.(10) is achieved;

$$\sigma_a\left(M_j,\alpha_k,t\right) \geq S(M_j,\alpha_k,t) \tag{10}$$

The earliest failure time of all locations, M_j, and directions, α_k, is defined as a failure time, t_f, of the glass plate. Fig.8 shows the flow chart of numerical simulation.

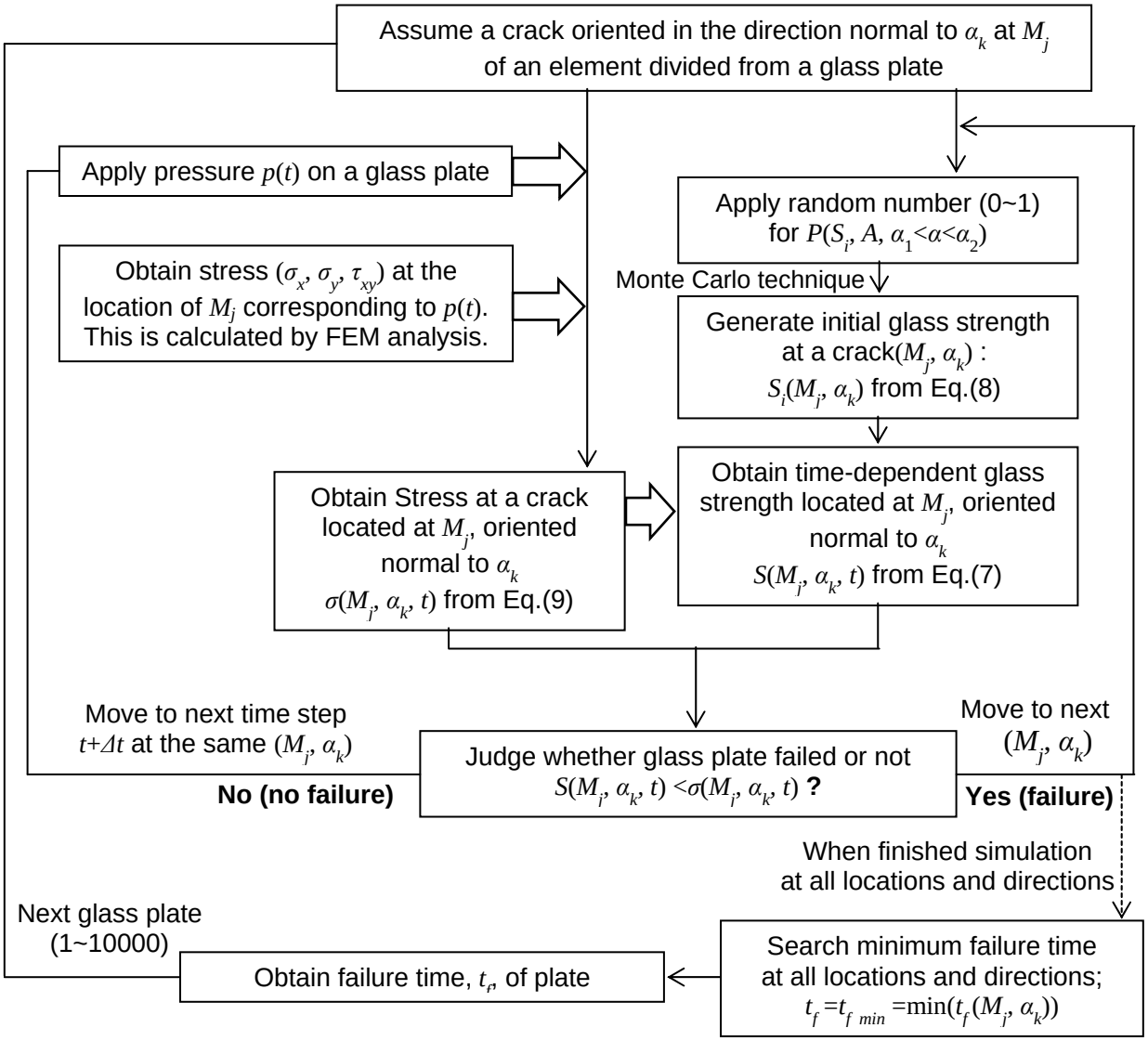

Fig.8 Flow chart of numerical simulation

3.2 INPUT DATA

In the present numerical simulation, a monolithic annealed glass plate of 855mm×790mm×3mm, which is the same as the one used for full-scale breakage tests, was assumed. The entire panel was divided into 225 element (M_j=M_1~ M_{225}) and each element contains a crack having 10 different directions with increments of $\pi/10$ (α_k=α_1 ~α_{10}). The considered loading patterns are two ramp loadings used in full-scale breakage tests.

Y, K_{IC}, K_{Ii} Geometrical shape factor, Y, and fracture toughness, K_{IC}, which are often used by previous researchers, were employed. Y=1.12 was selected as the one corresponding to a long single-ended crack in a semi-infinite solid. Concerning to K_{IC}, the value which corresponds to the one of a soda-lime silicate glass (K_{IC}=0.75) was utilized. In the present analysis, an initial stress intensity factor, K_{Ii}, is assumed to be equal to K_{IC}, in order to place the results from simulation firmly the safer side of design (Simiu and Reed 1983; 1984).

S_0, m S_0 and m were obtained by conducting ring-on-ring tests with small glass specimens and they are $S_0(1m^2)$=67.7 (MPa) and m=4.88. All the specimens used for the ring-on-ring tests were cut from the same glass plates used for the full scale brakeage tests, which are plates produced in same production line, delivered/preserved in same way.

A, n Coefficients A and n are related to crack growth. Their values vary depending on the environment such as humidity and temperature, and those obtained in a similar environment by different researchers also vary. In the present study, values of A and n employed by Kawabata(1996)(denoted as 'Case1') and Gavanski (2009)(denoted as 'Cases 2,3') for their numerical simulations, as shown in Table.2, were used.

Table.2 Summary of input parameters employed in the current numerical simulations

	Case1	Case2	Case3
$S_o(1m^2)$		67.7	
m		4.88	
K_{Ic}		0.75	
K_{Ii}		0.75	
Y		1.12	
A	3.46	1.08	1.08
n	16.64	16	19.69

$\sigma_x(M_j, t)$, $\sigma_y(M_j, t)$,$\tau_{xy}(M_j, t)$ Stress components at a location of M_j on glass plate surface were calculated by finite element method analysis (FEM analysis) using ABAQUS6.8.2. Fig.9 shows a modeling of elastic support condition in FEM analysis. In order to reduce calculation time, only 1/4 of the entire area of a square plate was modeled. Elastic-support was modeled by replacing gasket with spring. Rigidity of spring was decided based on the results of displacement measurement at the glass plate supported with gaskets using laser displacement transducers. However, the loads larger than 4kPa was not applied on the glass plate because there was a risk of breaking glass. Hence, a relationship between pressure and displacement above 4kPa

was not measured and hence was assumed as shown with a dotted line in Fig.10. Based on the applied pressure-displacement relationship, a relationship of pressure and rigidity of spring was determined as shown in Fig.11.

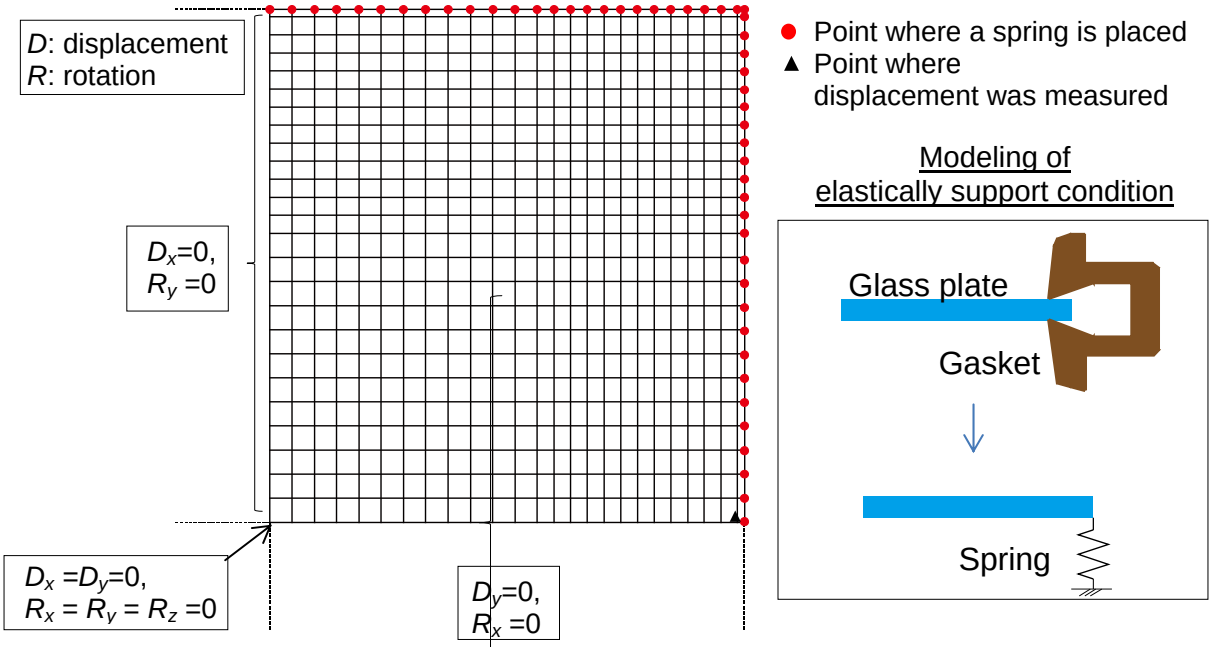

Fig.9 Modeling of glass plate in FEM

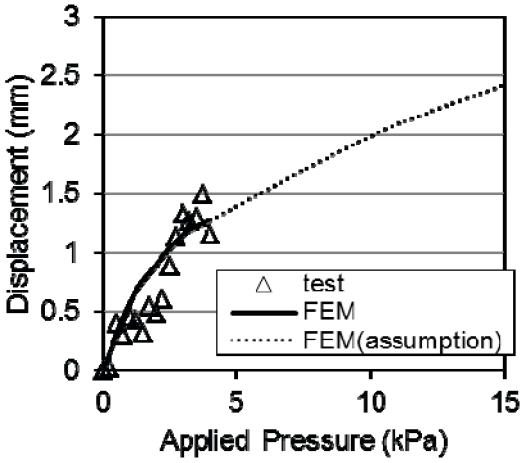

Fig.10 Relationship of pressure and displacement at edge of glass plate

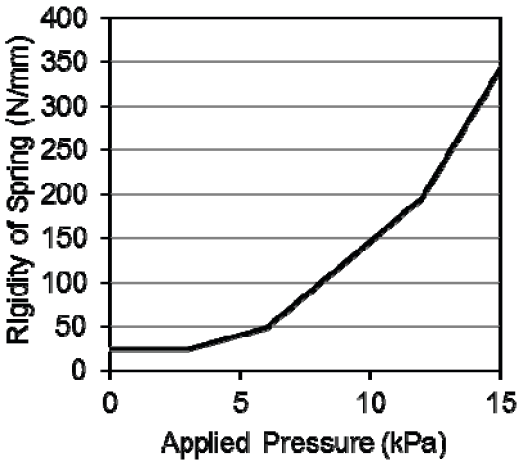

Fig.11 Relationship of pressure and rigidity of spring located at support points

3.3 EFFECT OF SUPPORT CONDITION

Fig.12 shows the cumulative distribution functions (CDFs) of failure pressures, p_f, obtained for the glass plates elastically supported and those simply supported in order to quantify the effect of support condition on glass failure pressure. As for the results for simple support condition, the modeling on FEM analysis is based on Gavanski (2009) and the input parameters used for numerical simulation are set as Case2 as shown in Table.2. It is found that the magnitude of failure pressure of elastic support is smaller than that of simple support, but there is no difference in their *COV*s (i.e., the shape of CDF is the same). This means that a different stress field on glass plates, which was caused by the difference in support conditions, seems to affect only failure pressure level but not its variation.

According to Kawabata (1996), the effect of support condition on the failure pressure varies depending on glass plate size. Hence, the relationship of the failure pressures between different glass plate support conditions obtained in the current can vary for different plate size.

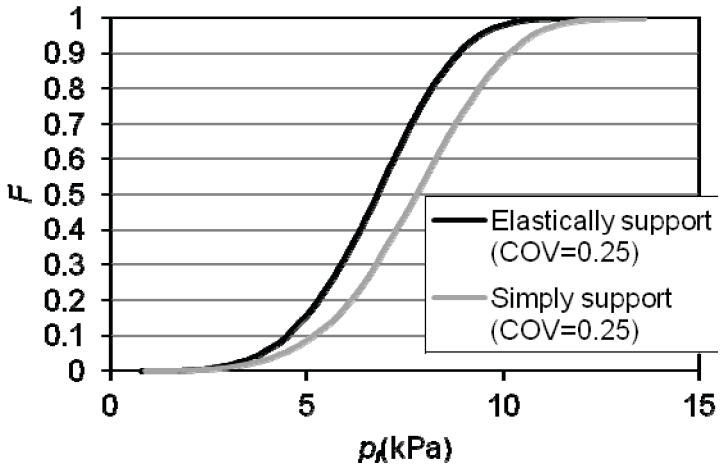

Fig.12 Comparison of CDFs of failure pressure obtained
with elastically support condition and simply support condition

3.4 COMPARISONS WITH FULL-SCALE BREAKAGE TEST RESULTS

Fig.13 shows comparisons between full-scale breakage test results (presented as “o” in the figure) and the numerical simulation results (presented as lines), for two ramp loading cases (16.4(Pa/sec) and 230(Pa/sec)). “Case3” of the numerical simulation relatively corresponds to the test results in both loading cases, compared to other two cases. However, further improvement is necessary, especially on the variation of failure pressure where the one of numerical simulation results is bigger than the one of test results.

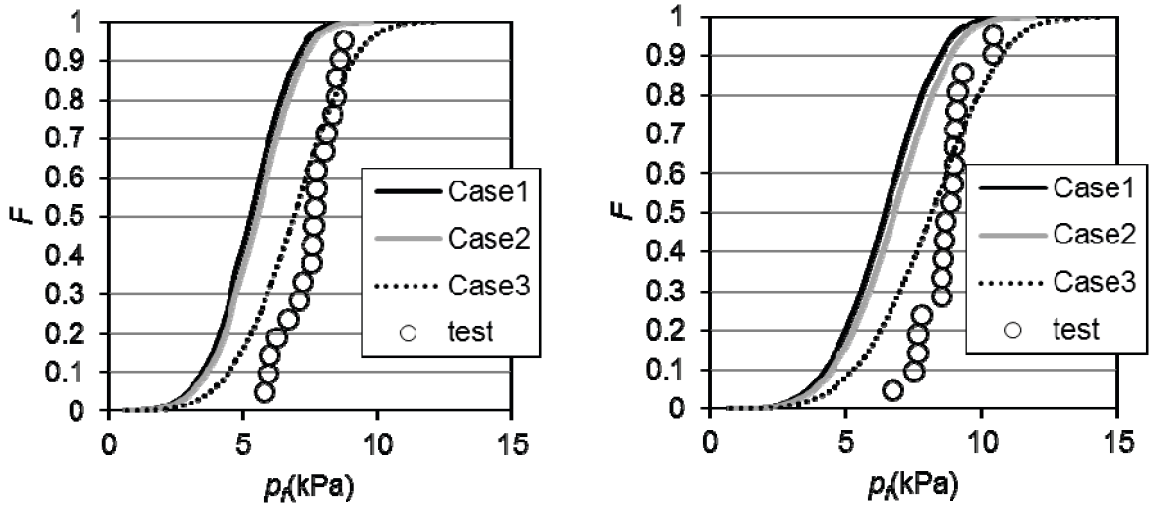

(a) Ramp1 (16.4(Pa/sec)) (b) Ramp2 (230(Pa/sec))

Fig.13 Comparisons with full-scale breakage test results

This difference in failure pressures is unlikely to have caused by the use of elastic support condition since it affects only the magnitude of failure pressure but not its COV as explained in 3.3. As shown in Table.2, since the input variable except *A* and *n* are the same among 3 cases considered in the numerical simulation, the effect of *A* and *n* must directly appear in Fig.13 and *n* seems to have the most influence on the simulation results. Hence, the influence of *A* and *n* on the numerical simulation results is further examined.

According to Simiu and Reed (1983; 1984), *A* and *n* represent the effect of temperature and humidity on glass strength. Hence, if the combination of *A* and *n* used in the current numerical simulation does not capture the environment where full-scale breakage tests were conducted, the disagreement between numerical simulation results and full-scale breakage test results is expected. However as explained in Section 3.2, the values of *A* and *n* obtained in the situation close to the present test condition are rather limited. Therefore, in the current study, a parametric study was conducted in order to clarify the effect of *A* and *n* on glass failure pressure in the range of the *A* and *n* values obtained by previous studies (0.1 to 50 for *A* and 15 to 25 for *n*).

Fig.14 shows the results when the value of *n* was varied. *A* was fixed to 1.08 and other parameters were set as shown in Table.2. It is found that both magnitude of failure pressure and its *COV* values increased as *n* increases and a small difference in *n* seems to have large effect on failure pressure. Even if *A* is set to other values, the trend found herein does not change.

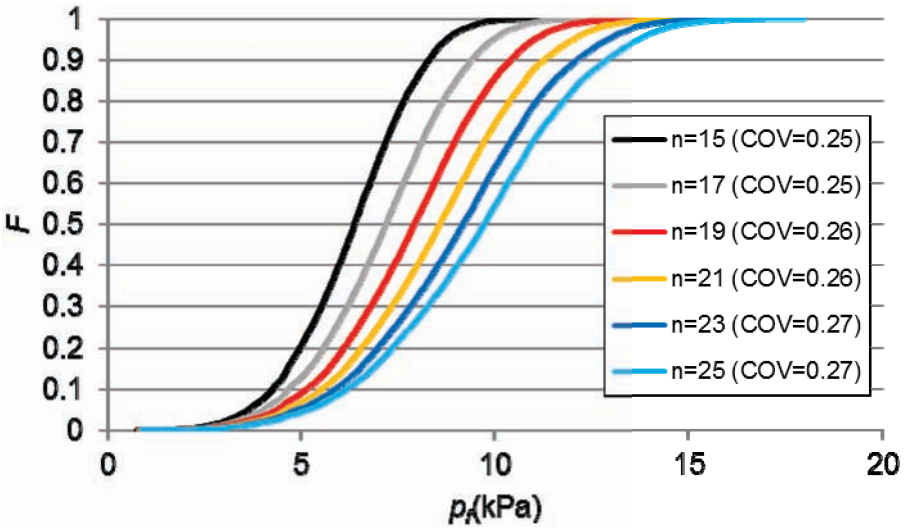

Fig.14 Effect of varying value of *n* on failure pressure

Fig.15 shows the results when the value of *A* was varied. *n* was fixed to 16 and other parameters are set as shown in Table.2. It is found that the magnitude of failure pressure increases as *A* decreases. However, *COV* is constant regardless of the value of *A* and this corresponds to the fact that the numerical simulation results of Cases 1 and 2 in Fig.13 are not much different. Even if *n* is set to other values, the trend found herein does not change.

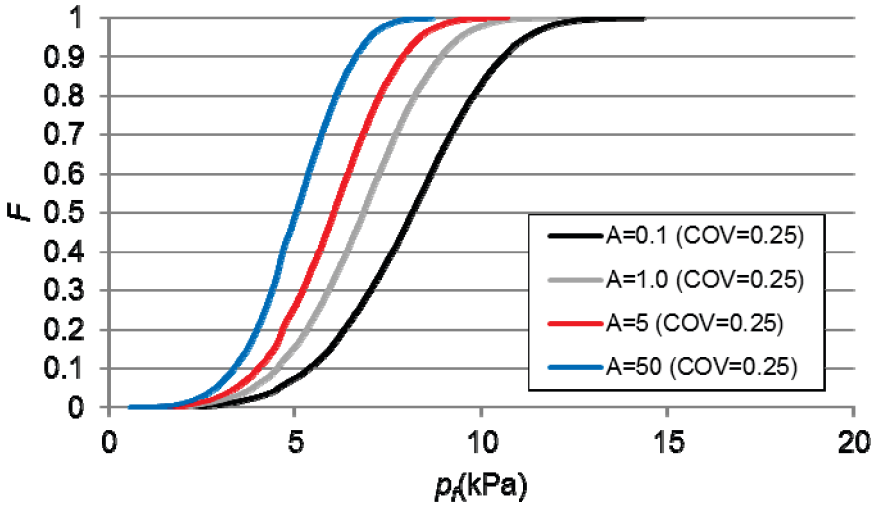

Fig.15 Effect of varying value of *A* on failure pressure

The fact that *A* affects only the magnitude of failure pressure but does not affect *COV* (show in Fig.16) of failure pressure can be a useful observation for capturing the effect of humidity on failure pressure in the numerical simulation. In the present full-scale breakage tests, it was hypothesized that the difference in failure pressure

levels obtained under ramp loadings and Dynamic loading was caused by the difference in humidity during the tests while there were no differences in *COV* of failure pressure. This fact indicates that humidity only affects the magnitude of failure pressure but not the COV of failure pressure. Considering the results of the parametric studies, *A* seems to be a parameter representing humidity and there is a possibility that the current numerical simulation can capture the difference in failure pressure caused by humidity by selecting the appropriate *A*. This will be examined in the forthcoming study.

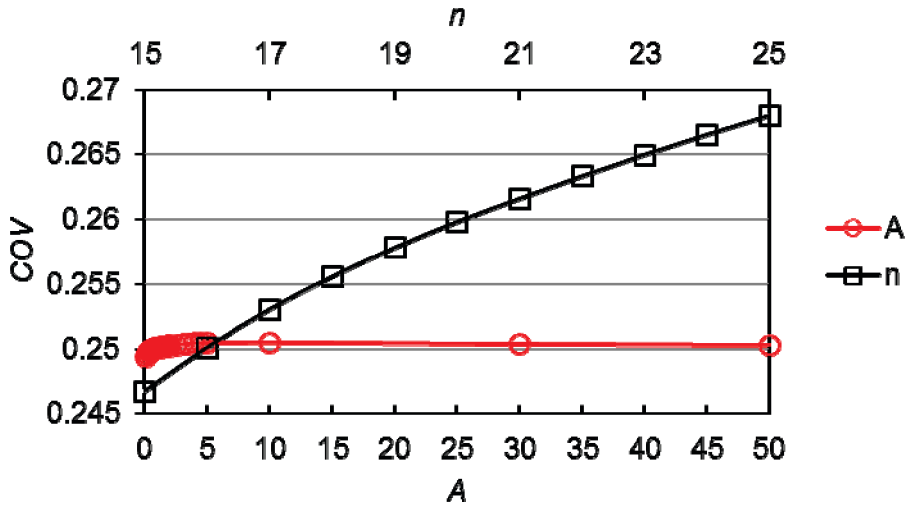

Fig.16 Effects of varying *A* and varying *n* on *COV* of failure pressure

Having understood the effect of both *A* and *n* on failure pressure, the combination of *A* and *n* which can capture the full-scale breakage test results was pursued. However, it was found that this is not possible unless *A* smaller than the value obtained by previous studies is employed if the other input variables are set as shown in Table.2. Among S_0, m, K_{IC}, K_{Ii} and Y, S_0 and m are believed to affect the numerical simulation results since they must be directly related to the conditions of ring-on-ring tests.

S_0 and m are initial strength parameters. They are Weibull parameters of initial strength, S_{i_ring}, which is obtained by converting failure stress from ring-on-ring tests considering the strength reduction due to static fatigue during the ring-on-ring tests. S_0 ($1m^2$) =67.7(MPa) and m =4.88 were obtained using the results of 25 specimens in the present study. Since the glass strength has a high variability, the obtained results can change significantly by changing the number of data used for the calculation of S_0 and m. This was examined in Fig.17 and Table.3. “No.2-No.25” means the smallest failure stress result among 25 results was eliminated for the calculation of S_0 and m. As seen in Fig.17, the Weibull distribution fit to the failure stress changes dramatically by changing the number of data and accordingly, the values of $S_0(1m^2)$ and m also change as shown in Table.3. This result indicates that the specimen number of 25 was not enough for the determination of stable S_0 and m and this may be a cause of the disagreement between numerical simulation results and the full-scale breakage test results.

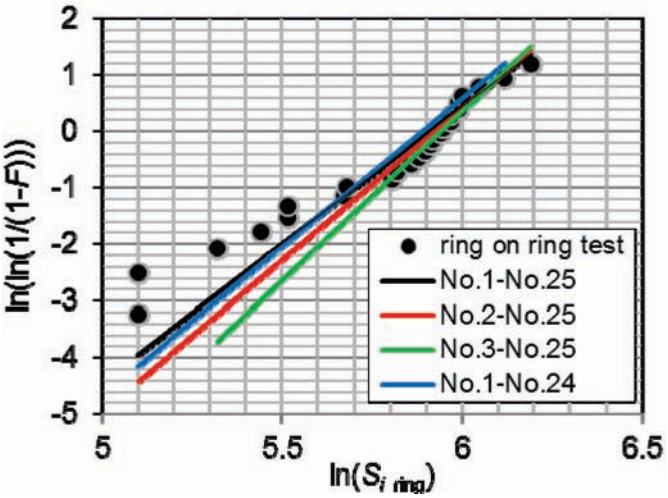

Fig.17 Weibull distribution fit
on initial glass strength from ring-on-ring test

Table.3
Weibull parameters for initial glass strength $S_0(1m^2)$ and m

Data used	$S_0(1m^2)$(Mpa)	m
No.1-No.25	67.7	4.88
No.2-No.25	80.1	5.37
No.3-No.25	95.6	5.99
No.1-No.24	75.0	5.26

4. CONCLUSIONS

In order to investigate the strength of elastically-supported glass plates subjected to wind load, full-scale breakage tests and numerical simulation which can predict glass failure pressure were performed.

In full-scale breakage tests, it was found that the results are consistent with the assumption that the damage accumulation of glass is independent of loading patterns when glass plates are elastically supported. In addition, humidity seems to affect the obtained failure pressures significantly.

The current numerical simulation could not predict full-scale breakage test results with enough accuracy and this was not because of the glass support condition but the other reasons. In order to clarify this cause, parametric studies on the parameters believed to affect the numerical simulation results were conducted. It was found that there is a limit in the modification of adjusting only the parameters of A and n, and it is necessary to consider the effect of initial strength. Based on the results of parametric study, a modification on the numerical simulation will be attempted.

5. ACKNOWLEDGEMENTS

All window glass plates utilized in the full-scale breakage tests were provided by YKK AP Inc.. E. Gavanski gratefully acknowledges research grant support from Japan Society for the Promotion of Science and Association for Disaster Prevention Research. The authors gratefully acknowledge the kind assistance of Mr. Satoru Maruyama, Mr. Tomoyuki Hatayama, Mr. Kazuyuki Sato and Mr. Junji Hayao of University Machine Service, Tohoku University who constructed the test apparatus. The authors also gratefully acknowledge Dr. Murray J. Morrison who developed the software for the Pressure Loading Actuator.

REFERENCES

Beason, W.L. (1980). "A failure prediction model for window glass." Ph.D. Thesis, Texas Tech. University, Lubbock, Texas.

Brown, W.G. (1972). "A load duration theory for glass design." *Pub. No. NRC* 12354, National Research Council of Canada, Ottawa.

Brown, W.G. (1974). "A practicable formulation for the strength of glass and its special application to large plates." *Pub. No. NRC* 14372, National Research Council Canada, Ottawa.

Dalgliesh, W.A. (1979). "Assessment of wind loads for glazing design." *Symp. on Practical Experiences with Flow-Induced Vibrations*, Karlsruhe, Germany, 696-708.

Gavanski E. (2009). "Behavior of glass plates under wind loads" Ph.D.Thesis,The University of Western Ontario,London,Ontario,Canada.

Holmes, J.D. (1985). "Wind action on glass and Brown‘s integral." *Eng. Struct.*, 7 (4), 226-230.

Kanabolo, D.C. and Norville, H.S. (1985). "The strength of new window glass plates using surface characteristics." Glass Res. and Testing Lab., Texas Tech. University, Lubbock, Tex.

Kawabata, S. (1996). "Study on wind resistance design of glass plate for cladding." Ph.D. Thesis, Nippon Sheet Glass Co. Ltd., Japan (in Japanese).

Ko, N.H., You, K.P., and Kim, Y.M. (2005). "The effect of non-Gaussian local wind pressures on a side face of a square building." *J. Wind. Eng. Ind. Aerodyn*., 93, 383-397.

Kopp, G. A., Surry, D., and Mans, C. (2005). "Wind effects of parapets on low buildings: Part 1. Basic aerodynamics and local loads." *J. Wind. Eng. Ind. Aerodyn*., 93(11), 817-841.

Kopp, G. A., Morrison, M. J., Gavanski, E., Henderson, D. J., and Hong, H. P. (2010). “Three little pigs” project: hurricane risk mitigation by integrated wind tunnel and full-scale laboratory tests. *Nat. Haz. Rev.*, 11(4), 151-161.

Li, Q.S., Calderone, I.J., and Melbourne, W.H. (1999). "Probabilistic characteristics of pressure fluctuations in separated and reattaching flows for various free-stream turbulence." *J. Wind. Eng. Ind. Aerodyn*., 82, 125-145.

Minor, J.E. (1981). "Window glass design practices: A review." *J. Struct. Div.,* 107(ST1), 1-12.

Miyoshi, S. (1964). "Wind pressure test on glass plate." *Summaries of technical paper of annual meeting* 100, Architectural Institute of Japan, 13-18.

Reed, D.A., and Simiu, E. (1984). "Wind Loading and strength of cladding glass." *J. Struct. Eng.*, 110 (4), 715-729.

Reed, D.A. (1993). "Influence of non-Gaussian local pressures on cladding glass." *J. Wind. Eng. Ind. Aerodyn*., 48(1), 51-61

Simiu, E., and Reed, D.A. (1983). "Probabilistic design of cladding glass subjected to wind loads." *4th Int. Conference on Applications of Statistics and Probability in Soil and Structural Engineering*, Universita di Firenze, Italy.

Wiederhorn, S.M. (1967). "Influence of water vapor on crack propagation in soda-lime glass." *J. Am. Ceram. Soc.*, 50 (8), 407-414.